International Journal of Thermophysics, Vol. 22, No. 4, 2001

Bidirectional Reflectance Distribution Function of Rough Silicon Wafers[1]

Y. J. Shen,[2] Z. M. Zhang,[2,3] B. K. Tsai,[4] and D. P. DeWitt[4]

The trend towards miniaturization of patterning features in integrated circuits (IC) has made traditional batch furnaces inadequate for many processes. Rapid thermal processing (RTP) of silicon wafers has become more popular in recent years for IC manufacturing. Light-pipe radiation thermometry is the method of choice for real-time temperature monitoring in RTP. However, the radiation environment can greatly affect the signal reaching the radiometer. The bidirectional reflectance distribution function (BRDF) of rough silicon wafers is needed for the prediction of the reflected radiation that reaches the radiometer and for reflective RTP furnace design. This paper presents the BRDF measurement results for several processing wafers in the wavelength range from 400 to 1100 nm with the spectral tri-function automated reference reflectometer (STARR) at the National Institute of Standards and Technology (NIST). The rms roughness of these samples ranges from 1 nm to 1 μm, as measured with an optical interferometric microscope. Correlations between the BRDF and surface parameters are obtained using different models by comparing theoretical predictions with experiments.

KEY WORDS: bidirectional reflectance distribution function (BRDF); radiometric temperature measurement; rapid thermal processing (RTP); silicon wafers; surface roughness.

1. INTRODUCTION

Reflectance of a rough or real surface is an important factor in many practical applications. Most apparently, the directional dependence of the

[1] Paper presented at the Fourteenth Symposium on Thermophysical Properties, June 25–30, 2000, Boulder, Colorado, U.S.A.

[2] Department of Mechanical Engineering, University of Florida, Gainesville, Florida 32611, U.S.A.

[3] To whom correspondence should be addressed. E-mail: zzhang@cimar.me.ufl.edu

[4] Optical Technology Division, National Institute of Standards and Technology, Gaithersburg, Maryland 20899, U.S.A.

0195-928X/01/0700-1311$19.50/0

radiative properties due to surface roughness can cause a significant error in radiative heat transfer calculations that employ specular or diffuse surface simplifications [1]. The effect of macroscopic roughness on the bidirectional reflectance distribution function (BRDF) has been applied to planet observations [2]. In the field of computer graphics, which deals with light reflection between objects, the current trends are to include the BRDF of real surfaces and to use physically based surface reflection models [3]. Furthermore, noncontact characterization of surfaces by scatterometry relies on BRDF measurements and relations between BRDF data and surface roughness parameters [4–7].

The motivation of the present study comes from our recent research on modeling the rapid thermal processing (RTP) chamber for radiometric temperature measurements [8, 9]. RTP is gradually replacing traditional batch furnaces in several key integrated circuit (IC) manufacturing processes, including annealing and oxidization [10]. The major barrier for implementation of RTP in many industrial processes is accurate radiometric temperature measurement, which requires the knowledge of the effective emissivity. Zhou et al. [11] have developed a Monte Carlo model to predict the effective emissivity according to the geometric arrangements and radiative properties of each surface within the RTP chamber. In this model, the reflectance of each surface consists of a specular component and a diffuse component. In many process systems, the silicon wafers are polished only on the front side, while the preferable arrangement is for the radiometer to view the rough side of the wafer. The reflectance of many real surfaces cannot be modeled simply by a specular component and a diffuse component. Because of the large amount of computational time often involved with Monte Carlo simulations, it is important to obtain suitable reflectance models for rough silicon wafers, which can correctly represent the BRDF data and be easily incorporated in Monte Carlo codes. This paper presents BRDF measurement results for several processing wafers and comparisons with available simplified models that are convenient for calculations.

2. EXPERIMENT

BRDF is a basic parameter for describing the nature of reflection for a surface element and is defined as [12–14]

$$f_r(\theta_i, \varphi_i; \theta_r, \varphi_r) = \frac{dL_r}{L_i \cos\theta_i \, d\omega_i} \qquad (\mathrm{sr}^{-1}) \tag{1}$$

where (θ_i, φ_i) and (θ_r, φ_r) denote the directions of incident and reflected beams, respectively, L_i is the incident radiance, and dL_r is the reflected radiance for radiation incident from an element solid angle $d\omega_i$. The geometry of the incident and reflected beams is shown in Fig. 1. The denominator of Eq. (1) is the incident irradiance. It is to be noted here that all the radiative properties discussed are spectral properties, which depend on the wavelength λ.

The measurements were performed using the spectral tri-function automated reference reflectometer (STARR) [13] in the Optical Technology Division at the National Institute of Standards and Technology (NIST). The STARR instrument can cover the spectral range from 200 to 2500 nm at angles of incidence from 0 to 80°, where the direction of reflection is constrained within the plane of incidence. Only measurements at wavelengths from 400 to 1100 nm, using a quartz-tungsten-halogen lamp and a silicon photodiode detector, are described here. The detector output signal is proportional to the radiant power reaching the detector. Hence, the BRDF is calculated by the following measurement equation:

$$f_r(\theta_i, \varphi_i; \theta_r, \varphi_r) = \frac{S_r}{S_i} \frac{1}{\cos\theta_r \, \delta\omega_r} \tag{2}$$

where S_r and S_i are the detector signals for the incident and reflected radiation; the ratio of S_r to S_i is a measure of the bidirectional reflectance, the solid angle $\delta\omega_r$ is approximately equal to A_r/D^2, where A_r is the aperture area of the detector, and D is the distance between the sample and the

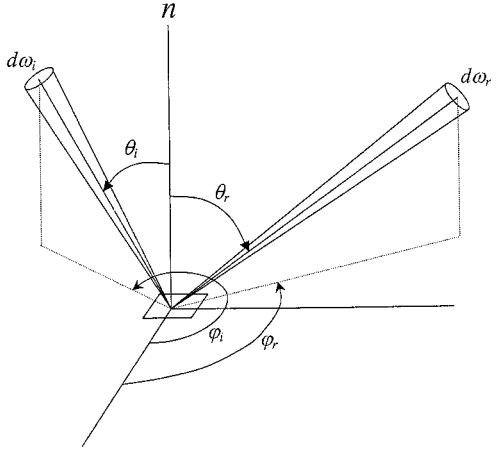

Fig. 1. Geometry of incident and reflected radiant beams.

detector. For the STARR, $A_r = 796.726\ \text{mm}^2$ and $D = 672.02$ mm, indicating that $\delta\omega_r = 0.0017642$ sr and the corresponding cone angle is 2.7°.

The other important property is the directional-hemispherical reflectance, which is related to the BRDF by

$$\rho_{dh}(\theta_i, \varphi_i) = \int_{2\pi} f_r(\theta_i, \varphi_i; \theta_r, \varphi_r) \cos\theta_r \, d\omega_r \tag{3}$$

The STARR also measures the directional-hemispherical reflectance at different wavelengths and at an incidence angle of 6°, using an integrating sphere. Utilizing the calibration with a white polytetrafluoroethylene (PTFE) plaque, the relative combined uncertainty ranges from 0.14 to 1.98% for the bidirectional reflectance measurements at wavelengths from 200 to 1600 nm when the reflection angle lies between 0 and 80°. The relative combined uncertainty for the directional-hemispherical reflectance measurements ranges from 0.21 to 0.67% for wavelengths from 200 to 1600 nm [13].

The sample surfaces were characterized with a scanning interference microscope system, TOPO-3D [15], in which interference fringes are produced when the light reflected off the reference mirror is combined with that reflected from the sample. The surface is profiled by scanning vertically, so that each point on the surface has an interference signal, and then locating the exact vertical position where each signal reaches its maximum amplitude [16]. The rms roughness averaged over three different spots ($606\ \mu\text{m} \times 461\ \mu\text{m}$ area) and their standard deviations are listed in Table I for four surfaces, labeled as A, B, C, and S. The surface images of surfaces A, B, and C are represented in Fig. 2. Surfaces A and B are the rough sides of two silicon wafers of 200 mm diameter and 0.8 mm thickness. These two surfaces may have been coated with oxide or nitride layers since their appearances are purple (surface A) and blue (surface B). Surface C is the rough side of a silicon wafer of 150 mm diameter and 0.6 mm thickness. A smooth surface, labeled S, is the polished side of the same wafer of surface B.

Table I. Sample Surfaces of Different Silicon Wafers

Surface label	A	B	C	S
Diameter (mm)	200	200	150	200
Wafer thickness (mm)	0.8	0.8	0.6	0.8
rms roughness σ	0.23 μm	0.13 μm	0.94 μm	1.08 nm
Standard deviation	0.003 μm	0.002 μm	0.04 μm	0.2 nm

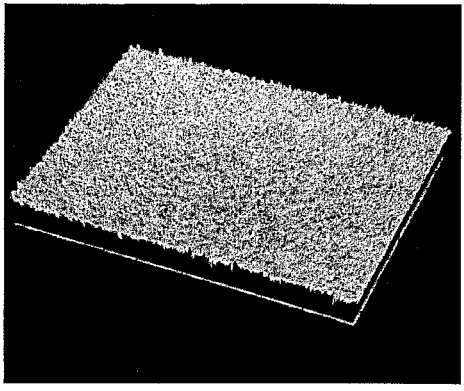

Surface A

Field size: 606 μm × 461 μm
rms roughness: 0.23 μm
Max. peak-valley distance: 4.97 μm

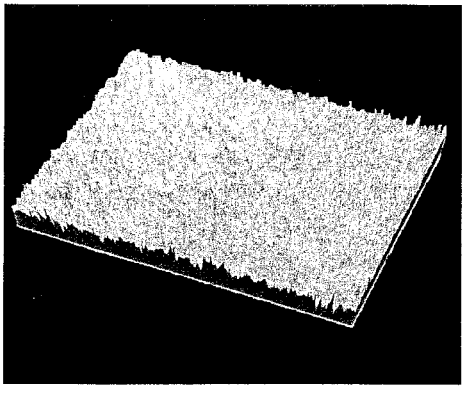

Surface B

Field size: 606 μm × 461 μm
rms roughness: 0.13 μm
Max. peak-valley distance: 2.14 μm

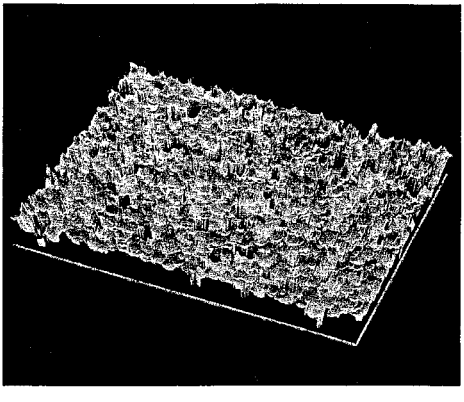

Surface C

Field size: 606 μm × 461 μm
rms roughness: 0.94 μm
Max. peak-valley distance: 7.74 μm

Fig. 2. Surface profiles for the three surfaces, A, B, and C.

3. RESULTS AND DISCUSSION

In the measurements, the reflected beam is constrained within the plane of incidence, i.e., φ_i and φ_r are related by either $\varphi_r = \varphi_i$ or $\varphi_r = \varphi_i \pm \pi$. Therefore, the BRDF data are presented in terms of an observation angle, defined as

$$\theta_{obs} = \begin{cases} \theta_r & \text{for} \quad \varphi_r = \varphi_i \pm \pi \\ -\theta_r & \text{for} \quad \varphi_r = \varphi_i \end{cases} \tag{4}$$

The measured BRDFs of surfaces A, B, and C at the wavelength of 950 nm are shown in Fig. 3 for incidence angles of 10 and 45°. The data represent the average values for p-polarization (where the electric field is parallel to the plane of incidence) and s-polarization (where the electric field is perpendicular to the plane of incidence). All curves are nearly symmetric about the specular angle, $\theta_{obs} = \theta_i$, where the BRDF is the greatest. In general, a rougher surface should show a lower specular reflection and a more uniform angular distribution due to surface scattering. Surface C, the roughest, clearly shows a much smaller BRDF value at the specular angle (more than an order of magnitude smaller than those of surfaces A and B). The angular variation of surface C is much smaller compared with other samples. In fact, the BRDF values, away from specular, for surface C are greater than those for surfaces A and B. It is interesting to note that for surface C, there exist subsidiary maxima at observation angles about 45° from the specular. Similar scattering results were seen for rough dielectric surfaces (due to multiple scattering) [17] and rough thin metallic films (due to the combined effect of multiple scattering and interference) [18]. The BRDF for surface B decreases most rapidly away from the specular angle, although the value at the specular angle for surface B is slightly smaller than that for surface A. The measured rms roughness for surface B is the smallest as expected. However, the abnormal behavior of the specular values indicates that the surface coatings may have affected the BRDF and roughness measurements. This is also shown by the measured directional-hemispherical reflectance of surface A, $\rho_{dh} = 0.81$, which indicates a possible coating effect.

The directional-hemispherical reflectance and the BRDF values at the specular angle for surface C are shown in Fig. 4 for $400 \text{ nm} < \lambda < 1100 \text{ nm}$. Notice that the directional emissivity is equal to $1 - \rho_{dh}$. The smooth curve in Fig. 4a is calculated from the Fresnel equations [14] using the refractive index (n) and extinction coefficient (κ) of silicon [19]. The measured ρ_{dh} agrees well with the theoretical values for smooth surfaces (except for $\lambda = 1100 \text{ nm}$). For dielectric materials, surface roughness has little impact on the emissivity, unless the specimen is semi-transparent or the roughness

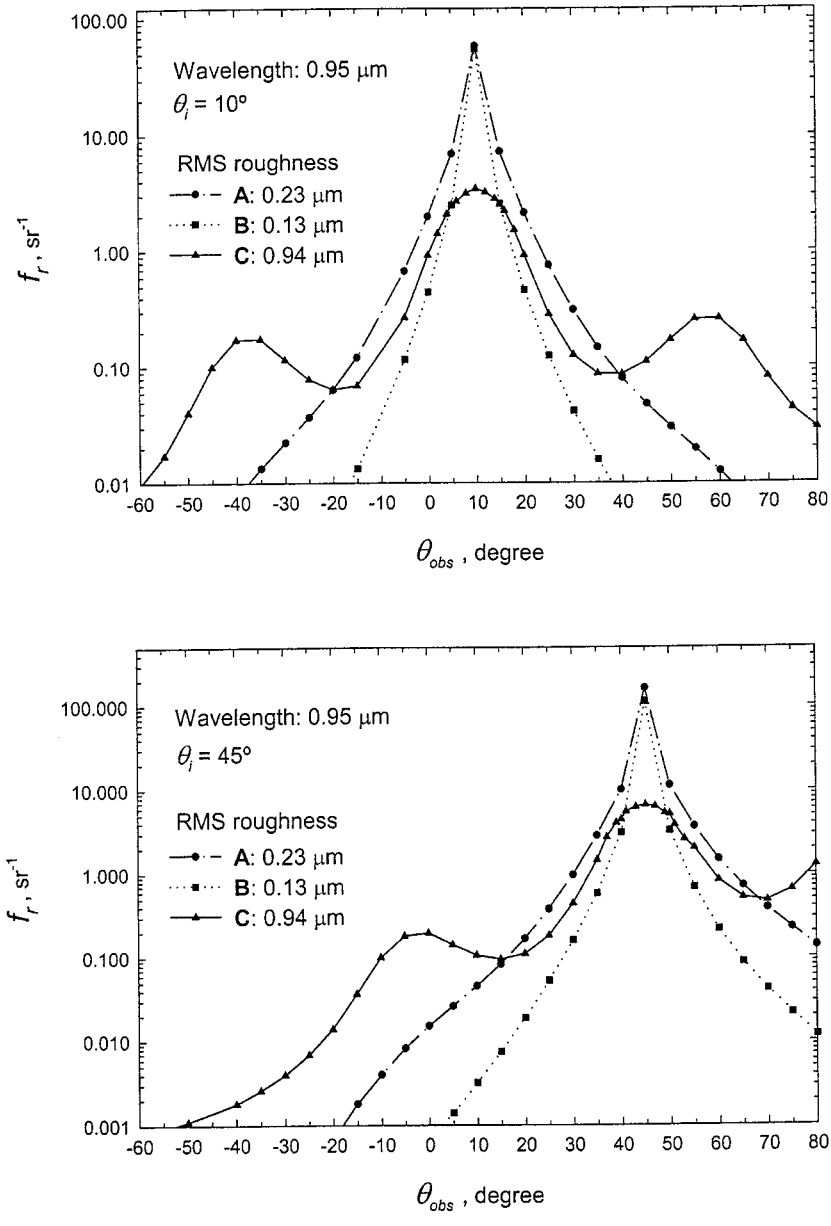

Fig. 3. Comparison of the measured BRDF at $\lambda = 0.95\,\mu$m at incidence angle of 10° (upper) and 45° (lower).

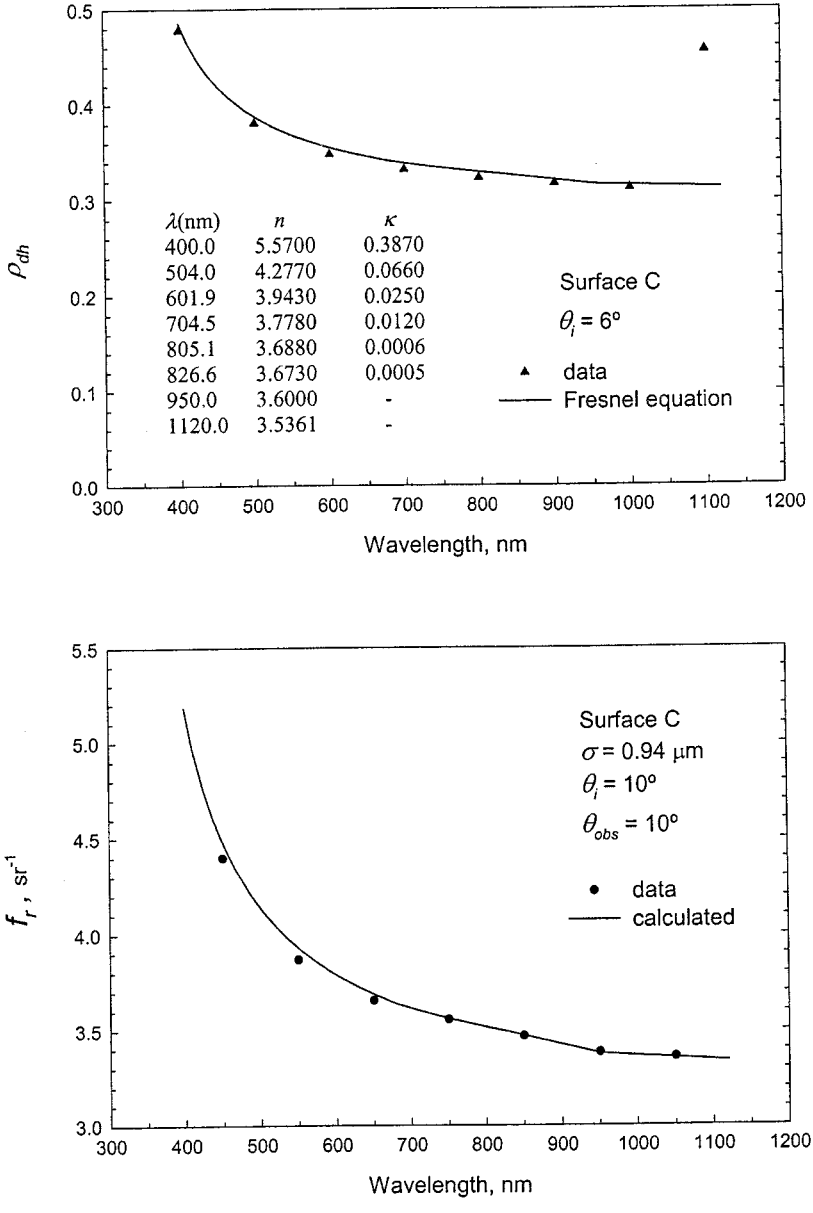

Fig. 4. Directional-hemispherical reflectance (upper) and BRDF at the specular angle (lower) for surface C.

is large enough to cause multiple scattering [20]. The larger ρ_{dh} measured at 1100 nm could be caused by the reflection from the other surface of the wafer since the absorption coefficient of silicon decreases rapidly as the wavelength is increased around 1100 nm (corresponding to the energy gap of silicon). In addition, the silicon diode used in these measurements almost reaches its detection limit at $\lambda = 1100$ nm, which may cause a large measurement uncertainty. In Fig. 4b, the calculated values are based on the Fresnel reflectance multiplied by a constant. In other words, the BRDF depends on the wavelength only through the refractive index and extinction coefficient. This is valid when the rms roughness is much greater than the wavelength as predicted by the theoretical models to be discussed in the next session. The constant is set to the ratio of the measured BRDF to the Fresnel reflectance at $\lambda = 950$ nm.

The BRDF data are employed to estimate the directional-hemispherical reflectance using Eq. (3). Since the BRDF data are limited within the plane of incidence, the assumption of an isotropic surface is made to perform the integration along the azimuthal direction. The calculated ρ_{dh} are 0.78, 0.27, and 0.53 for surfaces A, B, and C, respectively, whereas the measured values are correspondingly 0.81, 0.32, and 0.31. The large differences may be caused by the limited data used in the integration, especially near the specular direction, and the assumption of isotropic surfaces. The existence and shape of subsidiary maxima in the out-of-incidence planes of surface C should be further investigated.

Reflectance measurements for surface S were also made. The surface can be considered optically smooth and should be described by the Fresnel reflection equations. The measured specular reflectance at 10° incidence angle is 0.317 (averaged over $\rho_\perp = 0.322$ for s-polarization and $\rho_{||} = 0.312$ for p-polarization), which compares well with the theoretical value of 0.3195 ($\rho_\perp = 0.325$ and $\rho_{||} = 0.314$), calculated from the Fresnel equations with an estimated refractive index $n = 3.6$ at $\lambda = 950$ nm [19]. However, the measured specular reflectance is 0.288 ($\rho_\perp = 0.397$ and $\rho_{||} = 0.179$)) at 45° incidence angle, which is much smaller than the theoretical value of 0.3204 ($\rho_\perp = 0.444$ and $\rho_{||} = 0.197$). This unexpected large discrepancy needs further investigation.

4. COMPARISON WITH APPROXIMATE MODELS

Approximate models are selected to calculate the BRDF using a personal computer for a quick comparison with the experimental data. A review of various methods and approximations to describe wave scattering from rough surfaces can be found in Ogilvy [21]. Extensive theoretical and experimental investigations have been performed to obtain rigorous

electromagnetic-wave solutions and to determine the applicable regimes for each model [22–24]. The rigorous electromagnetic-wave solutions, however, are extremely computationally intensive. On the basis of simplicity and convenience for calculation, two approximate models are chosen and compared with the experimental results.

4.1. Davies Model

Davies [25] assumed a Gaussian distribution of heights of surface irregularities about the mean level and employed the Kirchhoff approximation to derive expressions for the electromagnetic energy reflected from rough surfaces. The Kirchhoff approximation is an extension of the Fresnel approximation that includes scattering but assumes that the radius of the surface curvature is smaller than the wavelength and that there is no multiple scattering [26]. The conditions for this approximation to be valid are: $\sigma/(a\cos\theta_i) < 0.2$ and $\sigma/\lambda < 2$ [22], where σ is the rms roughness and a is the surface autocorrelation length.

For slightly rough surfaces ($\sigma/\lambda \ll 1$), the BRDF includes a specular component and an off-specular component in this model. The specular component is expressed as

$$f_{r,s}(\theta_i, \varphi_i) = \frac{\rho_{dh,s}(\theta_i)}{\cos\theta_i \delta\omega_i} \exp\left[-\left(4\pi \frac{\sigma}{\lambda} \cos\theta_i\right)^2 \right] \tag{5}$$

and the off-specular component is calculated by

$$\begin{aligned} f_{r,off}&(\theta_i, \varphi_i; \theta_r, \varphi_r) \\ &= \frac{\rho_{dh,s}(\theta_i)}{\cos\theta_i \cos\theta_r} \pi^3 \left(\frac{a}{\lambda}\right)^2 \left(\frac{\sigma}{\lambda}\right)^2 (\cos\theta_i + \cos\theta_r)^4 \\ &\quad \cdot \exp\left\{ -\left(\frac{\pi a}{\lambda}\right)^2 [\sin^2\theta_i + \sin^2\theta_r + 2\sin\theta_i \sin\theta_r \cos(\varphi_i - \varphi_r)] \right\} \end{aligned} \tag{6}$$

where $\rho_{dh,s}$ is the directional-hemispherical reflectance for a smooth (specular) surface and is determined by the Fresnel equations. Considering the actual measurement conditions, the specular component, given by Eq. (5), exists in a finite solid angle around the specular direction [27]. Considering the solid angle in the measurement of the reflected radiation in the STARR instrument, we assume that the specular component contributes only in the range of specular angle $\pm 1.36°$.

The Davies model is also extended to very rough surfaces with $\sigma/\lambda > 1$ using the following expression,

$$f_r(\theta_i, \varphi_i; \theta_r, \varphi_r) = \frac{\rho_{dh,s}(\theta_i)}{\cos\theta_i \cos\theta_r} \frac{1}{16\pi} \left(\frac{a}{\sigma}\right)^2 \exp\left[-\left(\frac{a}{2\sigma}\right)^2 \cdot \frac{\sin^2\theta_i + \sin^2\theta_r + 2\sin\theta_i \sin\theta_r \cos(\varphi_i - \varphi_r)}{(\cos\theta_i + \cos\theta_r)^2} \right] \tag{7}$$

As seen in Eq. (7), for very rough surfaces, the wavelength dependence comes from the Fresnel reflectance only.

4.2. Torrance-Sparrow Model

Torrance and Sparrow [28] assumed that the rough surface consists of small, randomly disposed, mirror-like facets. This model is based on the geometrical-optics approximation, which neglects the phase of the electromagnetic wave. The applicable regions are approximately given by $\sigma \cos\theta_i/\lambda > 0.2$ and $\sigma/a < 2$ [23]. The equations for calculating the BRDF are rearranged in the following form [28, 29]:

$$f_r(\theta_i, \varphi_i; \theta_r, \varphi_r) = \frac{A}{\cos\theta_i} \left[\frac{g\rho_{dh,s}(\theta_d)\, G}{\cos\theta_r} \exp(-c^2\alpha^2) + \cos\theta_i \right] \tag{8}$$

where A, c, and g are constants related to the properties of facets and the solid angle of the incident beam, G is a masking and shading function and is equal to unity in the angle range considered in the present study, and the angles α and θ_d are related to θ_i, θ_r, φ_i, and φ_r through the fundamental spherical trigonometric relations [28]. When the reflected beam lies in the plane of incidence, $\alpha = (\theta_r - \theta_i)/2$ and $\theta_d = (\theta_i + \theta_r)/2$.

4.3. Comparisons

Comparisons between the measured data and model calculations for surfaces B and C are shown in Figs. 5 and 6, at $\lambda = 950$ nm and for $0° \leqslant \theta_r \leqslant 60°$. Because of the lack of accurate information, some parameters in the models are obtained by fitting the BRDF data. The fitting process, except for the specular data point in the slightly rough Davies model, is performed by an iterative algorithm, the Marquardt–Levenberg method [30], to obtain a convergent result. In the model for slightly rough surfaces, the off-specular component is fitted first, using Eq. (6), to obtain the roughness parameters a and σ. At the specular angle, the summation of the

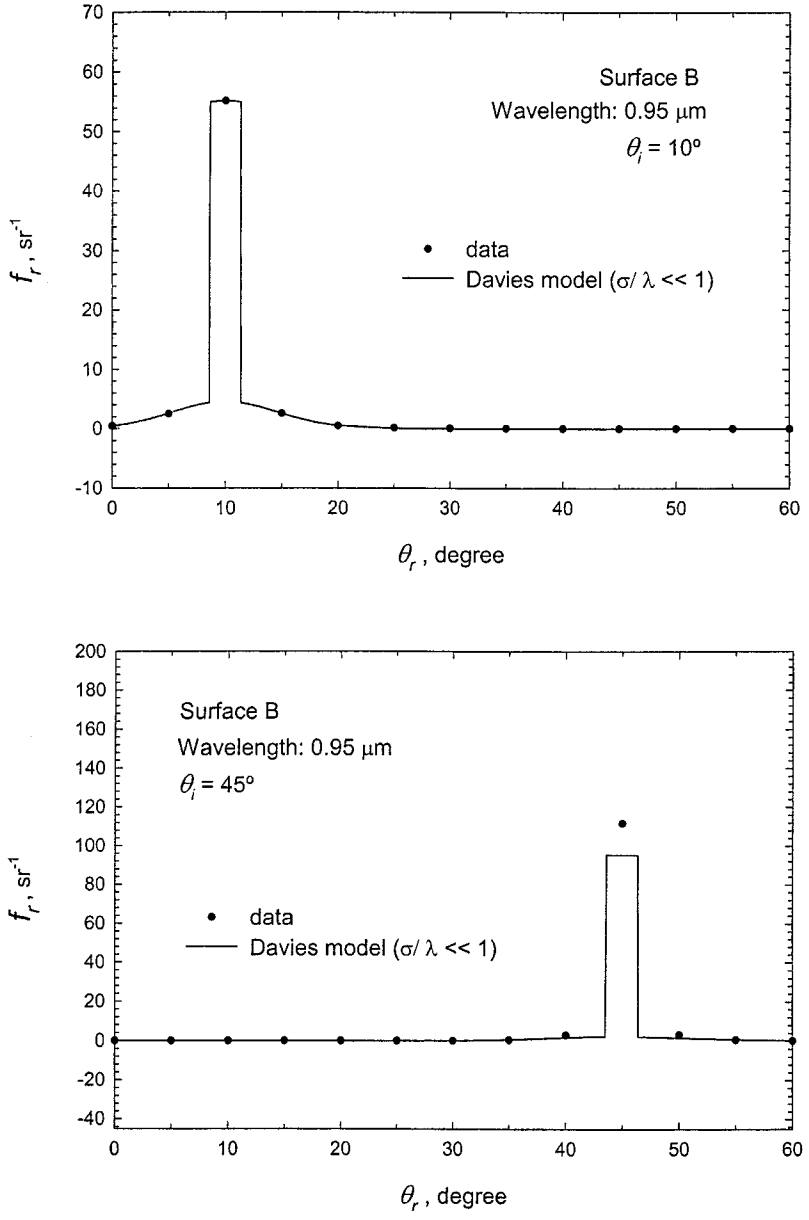

Fig. 5. Comparison of the Davies model with experiments for surface B: fitted result for 10° incidence angle (upper), and calculated result for 45° incidence angle (lower).

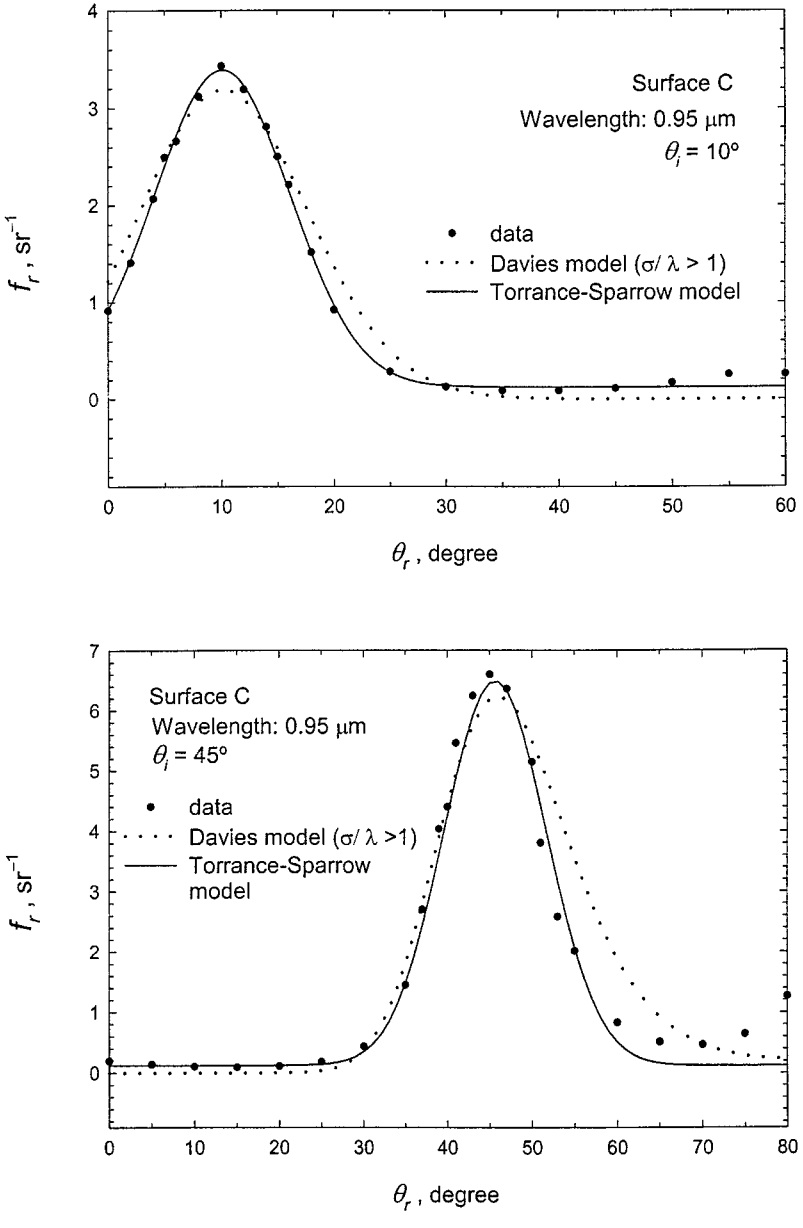

Fig. 6. Comparison of the Davies model and Torrance–Sparrow model with experiments for surface C: fitted results for 10° incidence angle (upper), and calculated results for 45° incidence angle (lower).

specular component, Eq. (5), and the off-specular component, Eq. (6), is fitted to the data point to obtain an additional parameter, $\delta\omega_i$, which was not known exactly in the experiments. Because the angular dependence of $\rho_{dh,s}(\theta)$ averaged over the two polarizations is small for $\theta \leqslant 45°$, it is assumed to be a constant, equal to 0.81 for surface A or 0.32 for surface B, in Eqs. (5)–(8) to simplify the fitting process. The fitting parameters for different models are listed in Table II.

For surface B, the Davies model for slightly rough surfaces is used to fit the measured data at a 10° incidence angle, as shown in Fig. 5a. The optimal fitting parameters obtained by fitting the data for the 10° incidence angle are then used to calculate the BRDF for the 45° incidence angle, as shown in Fig. 5b. The model approaches approximately the variation in BRDF data, but the relative difference in the calculated and measured values at the specular angle for the 45° incidence angle is 14.6%. The fitted σ is smaller than the measured value of 0.13 μm, and $\delta\omega_i$ is greater than $\delta\omega_r$. The surface coatings may have influenced the BRDF and roughness measurements; hence, the model considering pure silicon may not be suitable to predict the actual behavior. For surface A, the same model can be fit to the data approximately with different parameters using $\rho_{dh} = 0.81$, but the deviation is larger due to the possible coating effect. For surfaces A and B, good agreement could not be obtained using the Torrance–Sparrow model because the geometrical-optics approximation is applicable for relatively rough surfaces only.

For surface C, both the Davies model for rough surfaces and the Torrance–Sparrow model are fitted to the BDRF data at 10° incidence angle, as shown in Fig. 6a. The Torrance–Sparrow model can fit the data well for $\theta_r < 40°$, whereas the fitting results of the Davies model are not as good since there is only one adjustable parameter. At large reflection angles, the BRDF calculated from the Davies model approaches zero, while that calculated from the Torrance–Sparrow model approaches a constant, equal to A in Eq. (8). Both models failed to predict the subsidiary peaks

Table II. Values of Fitting Parameters

Surface	A	B	C	
Model	Davies (slightly rough)	Davies (slightly rough)	Davies (rough)	Torrance-Sparrow
Parameters	$\sigma = 0.07\ \mu$m $a = 2.2\ \mu$m $\delta\omega_i = 0.0078$ sr	$\sigma = 0.06\ \mu$m $a = 2.7\ \mu$m $\sigma w_i = 0.0036$ sr	$a/\sigma = 22$	$A = 0.124$ $c = 13.5$ $g = 80$

at about 45° from the specular angle. The same fitting parameters are used to calculate the BRDF for 45° incidence angle and compared with the data, as shown in Fig. 6b. Compared with the measured results, the curve calculated from the Torrence–Sparrow model is slightly shifted towards the right. This needs further investigation.

5. CONCLUSION AND FUTURE WORK

The BRDFs of several processing wafers, with rms roughness ranging from about 1 nm to 1 μm, have been measured at wavelengths from 400 to 1100 nm. Two simple models, categorized as the Kirchhoff approximation and the geometrical-optics approximation, are applied to fit the BRDF data. Reasonable agreement exists between the measured results and the model predictions without considering the coating effect. These simple formulae could be incorporated into the Monte Carlo model for rapid thermal processing systems to evaluate the effect of rough surfaces. Detailed surface characterization should be obtained to provide all the necessary parameters to correlate with the BRDF data. The effects of multi-layer coatings, polarization, and doping will be investigated in the future, and suitable models that include these effects will be developed to calculate the radiative properties of silicon.

ACKNOWLEDGMENTS

This work has been supported by the NIST Office of Microelectronics Program and the National Science Foundation (CTS-9875441). The authors thank P. Yvonne Barnes of NIST, Ferdinand Rosa, a former graduate student of the University of Florida, and Jorge Garcia for their assistance in the BRDF measurements.

REFERENCES

1. R. G. Hering and T. F. Smith, *Intl. J. Heat Mass Transfer* **13**:725 (1970).
2. B. Hapke, *Icarus* **59**:41 (1984); B. Hapke, *Theory of Reflectance and Emittance Spectroscopy* (Cambridge University Press, Cambridge, UK, 1993), Chap. 12.
3. D. P. Greenberg, K. E. Torrance, P. Shirley, J. Arvo, J. A. Ferwerda, S. Pattanaik, E. Lafortune, B. Walter, S.-C. Foo, and B. Trumbore, in *SIGGRAPH 97* (Association for Computing Machinery, Annual Conference Series, 1997), pp. 477–494.
4. J. C. Stover, M. L. Bernt, E. L. Church, and P. Z. Takacs, *Proc. SPIE* **2260**:182 (1994).
5. M. Bjuggren, L. Krummenacher, and L. Mattsson, *Opt. Eng.* **36**:874 (1997).
6. E. L. Church and P. Z. Takacs, in *Handbook of Optics, Volume I*, 2nd ed., M. Bass, ed. in chief (McGraw-Hill, New York, 1995), Chap. 7.

7. J. C. Stover, *Optical Scattering-Measurement and Analysis*, 2nd ed. (SPIE Optical Engineering Press, Bellingham, Washington, 1995), Chap. 4.
8. F. Rosa, Y. H. Zhou, Z. M. Zhang, D. P. DeWitt, and B. K. Tsai, in *Advanced in Rapid Thermal Processing*, F. Roozeboom, J. C. Gelpey, M. C. Öztürk, and J. Nakos, eds. (The Electrochemical Society, Pennington, New Jersey, 1999), Proc. Vol. 99–10, pp. 419–426.
9. Z. M. Zhang, *Annual Review of Heat Transfer*, C. L. Tien, ed. (Begell House, New York, 2000), Vol. 11, Chap. 6.
10. P. J. Timans, *Mat. Sci. Semicon. Processing* **1**:169 (1998).
11. Y. H. Zhou, Y. J. Shen, Z. M. Zhang, B. K. Tsai, and D. P. DeWitt, in *Proc. 8th Int. Conf. on Advanced Thermal Processing of Semiconductors* (RTP'2000), Gaithersburg, Maryland (2000), pp. 94–103.
12. F. E. Nicodemus, *Appl. Opt.* **9**:1474 (1970).
13. P. Y. Barnes, E. A. Early, and A. C. Parr, *Spectral Reflectance*, NIST Special Publication 250-48 (US Government Printing Office, Washington, DC, 1998); J. E. Proctor and P. Y. Barnes, *J. Res. Natl. Inst. Stand. Technol.* **101**:619 (1996).
14. M. F. Modest, *Radiative Heat Transfer* (McGraw-Hill, New York, 1993), Chap. 2.
15. WYKO Corp., Tucson, AZ. The identification within this paper of particular commercial equipment does not imply recommendation or endorsement by NIST, nor does it imply that the identified products are the best available for the purpose.
16. D. J. Whitehouse, *Meas. Sci. Technol.* **8**:955 (1997).
17. E. I. Chaikina, R. Hernández-Walls, and E. R. Méndez, *Proc. SPIE* **3141**:164 (1997); E. I. Chaikina, P. Negrete-Regagnon, G. Martínez-Niconoff, and E. R. Méndez, *Proc. SPIE* **3426**:153 (1998).
18. J. Q. Lu and A. A. Maradudin, *Proc. SPIE* **3141**:186 (1997).
19. D. F. Edwards, in *Handbook of Optical Constants of Solids*, E. D. Palik, ed. (Academic Press, Orlando, Florida, 1985), pp. 547-569.
20. P. J. Timans, in *Advances in Rapid Thermal and Integrated Processing*, F. Roozeboom, ed. (Kluwer Academic Publishers, Dordrecht, The Netherlands, 1996), Chap. 2.
21. J. A. Ogilvy, *Rep. Prog. Phys.* **50**:1553 (1987).
22. R. A. Dimenna and R. O. Buckius, *J. Thermophys. Heat Transfer* **8**:393 (1994).
23. K. Tang, R. A. Dimenna, and R. O. Buckius, *Int. J. Heat Mass Transfer* **40**:49 (1997).
24. D. W. Cohn, K. Tang, and R. O. Buckius, *Int. J. Heat Mass Transfer* **40**:3223 (1997).
25. H. Davies, *Proc. IEE* **101**:209 (1954); L.M. Spetner and H. Davies, *Proc. IEE* **102**C:148 (1955).
26. P. Beckmann and A. Spizzichino, *The Scattering of Electromagnetic Waves from Rough Surfaces* (Pergamon, New York, 1963), Chap. 3.
27. A. F. Houchens and R. G. Hering, *Prog. Astron. Aeron.* **20**:65 (1967).
28. K. E. Torrance and E. M. Sparrow, *J. Opt. Soc. Am.* **57**:1105 (1967).
29. J. G. Burnell, J. V. Nicholas, and D. R. White, *Opt. Eng.* **34**:1749 (1995).
30. W. H. Press, S. A. Teukolsky, W. T. Vetterling, and B. P. Flannery, *Numerical Recipes*, 2nd Ed. (Cambridge University Press, New York, 1992), Chap. 15.